# Cortical Bone Plate Properties Assessment using Inversion of Axially Transmitted Low Frequency Ultrasonic Guided Waves

Aubin Chaboty, Vu-Hieu Nguyen, Guillaume Haiat, Pierre Bélanger

Aubin Chaboty, École de Technologie Supérieure

# Cortical Bone Plate Properties Assessment using Inversion of Axially Transmitted Low Frequency Ultrasonic Guided Waves

Aubin Chaboty,[1] Vu-Hieu Nguyen,[2] Guillaume Haiat,[3] and Pierre Bélanger[1]

[1]*PULETS, École de Technologie Supérieure, Montréal, QC, Canada*[a]

[2]*MSME, CNRS UMR 8208, Univ Paris Est Creteil, Univ Gustave Eiffel, F-94010 Creteil, France*

[3]*MSME, CNRS, UMR 8208, F-94010 Créteil, France*

(Dated: 12 July 2024)

In the past few decades, early osteoporosis detection using ultrasonic bone quality evaluation has gained prominence. Specifically, various studies focused on axial transmission using ultrasonic guided waves and have highlighted this technique's sensitivity to intrinsic properties of long cortical bones. This work aims to demonstrate the potential of low-frequency ultrasonic guided waves to infer the properties of the bone inside which they are propagating. A proprietary ultrasonic transducer, tailored to transmit ultrasonic guided waves under 500 kHz, was used for the data collection. The gathered data underwent 2D Fast Fourier Transform processing to extract experimental dispersion curves. The proposed inversion scheme compares experimental dispersion curves with simulated dispersion curves calculated through the semi-analytical iso-geometric analysis (SAIGA) method. The numerical model integrates a bone phantom plate coupled with a soft tissue layer on its top surface, mimicking the experimental bone phantom plates. Subsequently, the mechanical properties of the bone phantom plates were estimated by reducing the misfit between the experimental and simulated dispersion curves. This inversion leaned heavily on the dispersive trajectories and amplitudes of ultrasonic guided wave modes. Results indicate a marginal discrepancy under 5% between the mechanical properties ascertained using the SAIGA-based inversion and those measured using bulk wave pulse-echo measurements.

[a]aubin.chaboty.1@ens.etsmtl.ca

## I. INTRODUCTION

Osteoporosis is a skeletal disorder characterized by compromised bone strength, leading to an increased risk of fracture[1,2]. The early diagnosis of osteoporosis is crucial as it allows for timely intervention and prevention of fractures, and it has been extensively studied in the past few decades. Bone density measurement is the gold standard to diagnose the disease. However, the comprehensive evaluation of a person's bone health and fracture risk should ideally consider other characteristics such as the bone stiffness, the cortical thickness and/or the bone volume fraction[3–5].

Osteoporosis is generally more prevalent in postmenopausal women, with nearly one in two women affected (40%). It can also be found in 15% to 30% of the over 50 years old male population for a combined total of approximately 200 million people affected worldwide[6–9]. Comparatively, one in ten people will develop a cancer, across all ages, and the risk to develop a cardiovascular disease is near 50%[10,11]. Osteoporosis constitutes a major threat to healthcare systems and leads to significant hospitalization costs worldwide. It is estimated that there will be nearly 6.3 million hip fractures per year around the world by 2050, representing several billion dollars in healthcare costs[4]. Early detection of osteoporosis is crucial to prevent fracture risk.

Recognized as the gold standard for diagnosing osteoporosis, dual-energy x-ray absorptiometry (DEXA) uses two X-rays of different energy levels to estimate the bone density, allowing to retrieve a 2D information on the bone mineral density (BMD)[12,13]. To diagnose osteoporosis in a patient, BMD is expressed in terms of standard deviation from a population

of healthy young adults called the T-score[14]. According to the World Health Organization, a T-score of -2.5 or lower is considered as confirmed osteoporosis. The success of DEXA lies in the fact that this technology and the interaction of X-rays with bones are well understood and known[15]. Although this technology allows for obtaining BMD for different sites in the human body, it remains difficult to retrieve the bone mechanical properties. The poor sensitivity of BMD measurements makes the monitoring of the disease's progression difficult to be carried out in the clinic. Moreover, DEXA is relatively expensive to implement and requires adequate infrastructure.

Quantitative ultrasound (QUS) methods have been introduced as nonionizing alternatives. The main motivation for the use of ultrasound lies in its ability to assess bone mechanical properties, ultrasonic wave speed and attenuation being affected by the medium of propagation[16], which allows to go beyond a simple BMD (Bone Mineral Density) estimation[4,5,15,17,18]. QUS techniques have the advantage of being simple, safe, and cost-effective. However, it should be noted that there is a lack of standardized quality control and a great heterogeneity in the technologies used, making the results obtained by different devices difficult to compare. The most widely QUS techniques used in the clinic are transverse and axial transmission devices.

Ultrasonic guided waves are widely used in the field of nondestructive testing to characterize materials such as composite or bonded plates, for example[19–23]. This method has been adapted in recent years for cortical bones[24,25]. Axial transmission uses ultrasonic guided waves and is sensitive to intrinsic properties of cortical bone. This method is applied to long bones such as the tibia, radius, or femur[26–29]. The clinical significance of ultrasound

velocities in reflecting various aspects of bone strength, such as cortical thickness, stiffness, and porosity, has been partially confirmed. The initial studies on axial transmission were primarily focused on measuring the time-of-flight (TOF) of the first arriving signal (FAS)[30]. The velocity of the fastest wave mode was then calculated and his typically associated with the fundamental symmetrical mode of a plate[31]. Several clinical studies demonstrated that the FAS velocity can be used to distinguish healthy from osteoporotic individuals[29,32,33].

However, assessing the mechanical and geometrical properties of bone cortical tissue using ultrasonic guided waves involves the complex issue of solving multiparametric inverse problems[3,18]. This resolution process relies on inversion algorithms that attempt to match experimental data with simulated dispersion curves of ultrasonic guided wave modes, computed for simplified models such as plates or cylinders[34,35]. In previous studies, two approaches were proposed: operating at low frequencies (<500 kHz) and high frequencies (>1 MHz).

Low-frequency guided waves can penetrate more deeper inside cortical bone due to lower attenuation and longer wavelengths. This ability to assess bone in its volume makes them potentially useful to determine bone thickness, particularly in the early stages of osteoporosis when the endosteal region is primarily affected[36]. Moilanen et al.[37] introduced an inversion scheme using a free isotropic plate model to estimate the cortical thickness of phantom plates, which was later applied to tubular structures and ex-vivo bones[35,38]. Similarly, Ta et al.[39] used a hollow isotropic cylinder filled with a viscous liquid to determine the thickness of bovine tibia specimens by manually matching experimental velocities with the phase velocities of simulated modes. Pereira et al.[40] studied the interaction of very low frequency (20-40

kHz) ultrasonic guided wave modes with an irregular, multi-layered, and heterogeneous bone cross-section modeled with anisotropic and viscoelastic material properties. Their results indicated that the FAS is not a good discriminator of intracortical bone properties, highlighting the need to target specific modes and not only the FAS to access bone properties. Consequently, low-frequency methods face limitations, including the challenge of retrieving multiple bone parameters beyond cortical thickness due to the limited information contained in the few low-order modes typically utilized. Defining the appropriate operating frequency range remains a key challenge in low-frequency assessments.

Higher frequencies are more likely to retrieve several parameters of the bone cortex through inverse scheme. At these frequencies, the bone shape can be approximated by a plate-like structure. Foiret et al.[41] presented an inverse characterization method to estimate both the thickness and bulk wave velocities of *ex-vivo* cortical bone samples, using a transverse isotropic free plate model with a user-parameter-dependent algorithm. Subsequently, the same research group utilized inversion schemes based on genetic algorithms to extract information from a multimode dataset, without the necessity of prior knowledge regarding the mode orders[34]. Several studies have highlighted the complexity introduced by the presence of soft tissues when extracting dispersion curves, leading to a larger number of modes and higher attenuation[42–44]. More recently, a bilayer plate model was introduced to explore the accuracy of the inversion method when dealing with more complex models and the presence of soft tissue[3]. Results indicated that while the free plate model (without the soft tissue layer) allows for reliable retrieval of waveguide properties, the bilayer model could become unmanageable for solving the inverse problem due to the additional modes

induced by the soft tissue layer. Li et al.[45] later introduced deep neural networks to replace traditional inverse algorithms for better estimation of cortical parameters. Despite the potential to simplify the model geometry, higher frequencies may present significant challenges in managing the inverse problem due to the numerous modes generated, which can accommodate almost any set of model parameters.

The originality of the present method lies in using low-frequency guided waves (from 50 kHz to 500 kHz) to retrieve the cortical thickness and properties of phantom plates topped with soft tissue, employing a bilayer model representative of the experimental samples. This frequency range reduces the number of propagating modes despite the presence of soft tissue, thereby increasing the accuracy of the proposed inverse method. Additionally, Pereira et al.[46] demonstrated that using the amplitude of ultrasonic guided wave modes can significantly enhance the accuracy of the inversion, although their model did not account for soft tissue. Thus, incorporating an excitability value into the inversion process of the proposed method ensures that the inversion is based on both the dispersive properties of ultrasonic guided waves and their amplitude, making the model sensitive to both cortical thickness and cortical properties.

This paper aims to simulate a parameterized cortical bone phantom plate with a soft tissue layer using the semi-analytical iso-geometric analysis (SAIGA)[47,48] to perform the inverse characterization of the mechanical and the geometrical properties of soft tissue covered bone phantom plates. Two cortical phantom plates coupled with a soft tissue mimicking layer were used experimentally. A proprietary ultrasonic transducer specifically designed to excite ultrasonic guided waves under 500 kHz was used for measurements. Acquired data

were processed using the 2D Fast Fourier Transform to extract the dispersion curves of the propagating modes. The curves were then compared with the semi-analytical predictions. For both plates, five parameters were estimated using the inversion scheme: (1-2) the longitudinal and shear velocities in the cortical layer; (3-4) thicknesses of both layers; and (5) the sound velocity in the soft tissue layer. To ensure that the inversion between simulated and experimental dispersion curves was based on the dispersive properties of ultrasonic guided waves and their amplitudes, excitability of the different guided wave modes is taken into consideration in the cost function.

## II. MATERIAL AND METHODS

### A. Models and Simulations Models

A numerical model comprising a bone phantom plate coupled with a soft tissue layer, mirroring experimental bone phantom plates, was used to match experimental dispersion curves with ultrasonic guided wave modes calculated by SAIGA[47,48]. Solving SAIGA equations enables the calculation of modes as well as their amplitude. Section II A 1 describes the plate like model used as a forward model in this study. Section II A 2 then summarizes background of the SAIGA method and detailed the formulation of the mode excitability used.

### 1. *Plate-like Model*

The model geometry was defined based on the experimental bone phantom plates. Consider a homogeneous isotropic solid layer ($\Omega^S$) of infinite extend and constant thickness $h^S$ in the direction of propagation ($e_1$). The upper surface of the solid layer is loaded with soft tissue layer ($\Omega^f$) modeled as fluid of thicknesses $h^f$. Fig. 1(a) shows a description of the model's geometry.

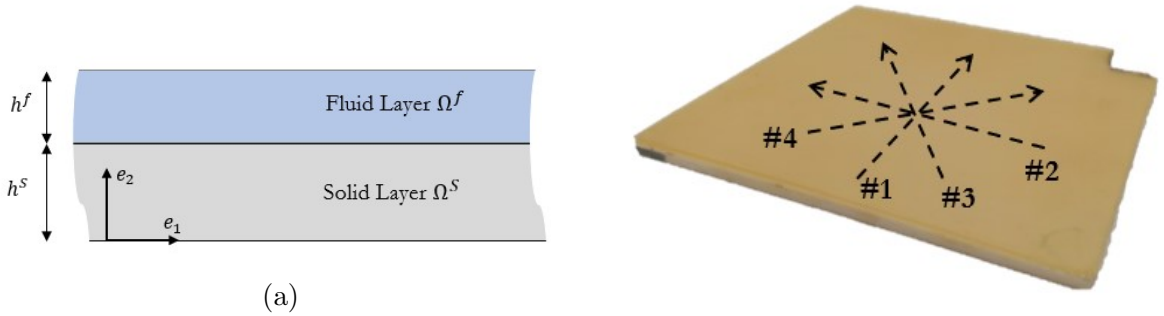


(a) (b)

FIG. 1. (a) Geometry description of the cortical solid layer topped by a fluid finite space. (b) Experimental bone phantom plates with the four different directions of axial transmission measurements.

The cortical layer of the waveguide was modeled as a homogeneous viscoelastic medium defined by its density ($\rho$), its Young's modulus ($E$) and Poisson's ratio ($\nu$). Longitudinal and shear velocities of the solid layer are then derived from these parameters and used for the inversion process. This enable the respect of thermodynamic laws and avoid having results which have no physical meaning or values too far away from those found in the literature[49–54]. The resulting model parameters, which reflect the waveguide's stiffness, consist of two bulk waves velocities $C_P$ and $C_S$, incorporating the mass density within

the velocity parameters[3,17,18,55], and a stiffness ratio of elastic coefficients $C_{11}/C_{13} = 1 - 2(C_S/C_P)^2$. For the longitudinal and shear waves, two attenuation coefficients $\alpha_P$ and $\alpha_S$ were added to the model and used for the calculation of the viscoelastic tensor. The ratio between $\alpha_S$ and $\alpha_P$ at a frequency of 1 MHz was fixed at 1.5[56,57], with $\alpha_P = 2.9$ dB/cm at this frequency in accordance with the manufacturer properties. Therefore, viscoelastic tensor coefficients can be calculated as[58,59]:

$$\eta_{11} = \eta_{22} = \frac{\alpha_P}{8.686} \times 2C_P \times \frac{C_{11}}{(\omega_{ref})^2} \tag{1a}$$

$$\eta_{33} = \frac{\alpha_S}{8.686} \times 2C_S \times \frac{C_{33}}{(\omega_{ref})^2} \tag{1b}$$

$$\eta_{12} = \eta_{11} - 2 \times \eta_{33} \tag{1c}$$

where $\omega_{ref} = 2\pi.f_{req}$ with $f_{req} = 1$ MHz the reference frequency used for the calculation of the viscoelastic tensor. The values of $\eta_{11}$, $\eta_{33}$ and $\eta_{12}$ are assumed to be constant within the frequency bandwidth of interest and determined by the value of the attenuation coefficients at frequency $f_{req}$. The effective stiffness tensor was then express as a complex tensor $C_{eff} = C + i\eta\omega_{ref}$. In the same way, the soft tissue layer was model as a fluid with its density ($\rho^f$), its sound velocity ($C^f$), and its attenuation coefficient $\alpha_f = 0.6$ dB/cm at 1 MHz, with its bulk modulus $K = \rho^f(C^f)^2$ and its viscoelastic coefficient $\eta^f = \frac{\alpha_f}{8.686} \times 2C^f \times \frac{K}{(\omega_{ref})^2}$. NURBS basis functions of order 8 were used for the SAIGA analysis. Three patches were used in each layer so that the number of degrees of freedom $N_{Dof} = 33$. Dispersion curves were computed within a frequency range from 50 to 500 kHz at a step of 5 kHz.

### 2. *Semi-Analytical Iso-geometric Analysis (SAIGA) Method*

The SAIGA method uses the same principle as the semi-analytical finite element (SAFE) method[60–62], but instead of using Lagrange polynomials for approximation, SAIGA uses B-splines and non-uniform rational B-Splines (NURBS) basis functions, providing higher continuity across the element boundaries, therefore significantly improving the precision, and reducing the computational cost[63,64]. To determine the dispersion of guided waves, the method considers the waves propagating harmonically in the axial direction ($e_1$), which can be expressed for the displacement $\mathbf{u}$ and the acoustic pressure $\mathbf{p}$ as follows:

$$\boldsymbol{u}(x_1, x_2, t) = \mathbf{U}(x_2)e^{i(k_1 x_1 - \omega t)} \tag{2a}$$

$$\boldsymbol{p}(x_1, x_2, t) = \mathbf{P}(x_2)e^{i(k_1 x_1 - \omega t)} \tag{2b}$$

where $\omega$ is the angular frequency, $t$ is the time, $k_1$ is the wave number in the propagation direction ($e_1$), vector $\mathbf{U}(x_2) = (U_1, U_2)^T$ and $\mathbf{P}(x_2) = P$ are respectively the amplitude of displacement in the solid domain $\Omega^S$ and pressure in the fluid domain $\Omega^f$. Essentially, employing SAIGA method leads to a quadratic eigenvalue problem to be solved for determining the relationship between the wavenumber ($k_1$) and angular frequency ($\omega$). It could be solved with respect to $k_1$ as follows:

$$(-\omega^2\mathbf{M} + \mathbf{K}_0 + ik_1\mathbf{K}_1 + k_1^2\mathbf{K}_2)\mathbf{V} = \mathbf{0} \tag{3}$$

where $\mathbf{V} = (\mathbf{P}, \mathbf{U})^T$ contains the global eigenvectors of pressure ($\mathbf{P}$) and of displacement ($\mathbf{U}$), and $\mathbf{M}, \mathbf{K}_0, \mathbf{K}_1, \mathbf{K}_2$ are the global matrices of the system. More details can be found in the work of Seyfaddini and al.[47,48]. By solving Eq. (3), it is possible to determine the

eigenvalues $k_1$ and the corresponding eigenvectors $\mathbf{V}(\omega, k_1)$ of guided modes for each value of angular frequency $\omega$. The frequency dependent phase velocity ($C_{ph}$) and the attenuation ($att$) can be determined by:

$$C_{ph} = \omega/\Re(k_1)\ m/s \qquad att(\omega) = \Im(k_1)\ Np/m \tag{4}$$

To ensure that the inversion between simulated and experimental dispersion curves was based on the dispersive properties of ultrasonic guided waves and their amplitudes, the excitability $Ex$ of a given mode was calculated based on its mode shape as:

$$Ex(k_1, \omega) = \frac{\Re(k_1, \omega)}{\Im(k_1, \omega)} \times U^2_{norm}(k_1, \omega) \tag{5a}$$

$$U_{norm}(k_1, \omega) = \frac{abs(U_{2,surf})}{max(U_{1S}, U_{2S}, U_{1f}, U_{2f})} \tag{5b}$$

where $U_{1S}$, $U_{2S}$, $U_{1f}$, $U_{2f}$ are respectively the in plane and out of plane displacement in the solid layer, and the in plane and out of plane displacement in the top fluid layer. $U_{2,surf}$ is the out of plane displacement at the top surface. An example of the excitability of guided wave modes in the bi-layer model as a function of frequency is displayed in Fig. 2(a). The color of each circle denotes the amplitude of the mode excitability associated with each mode. Fig. 2(b) represents the mode shapes associated with the selected mode on Fig. 2(a), with the different displacement used in the calculation of excitability.

### B. Inversion scheme

It was assumed that matching experimental dispersion curves with the semi-analytical predictions generated via SAIGA may serve as a methodological approach for deducing the cortical bone properties (velocities $C_P$ and $C_S$, thickness $h^S$) of the plate's solid layer. In

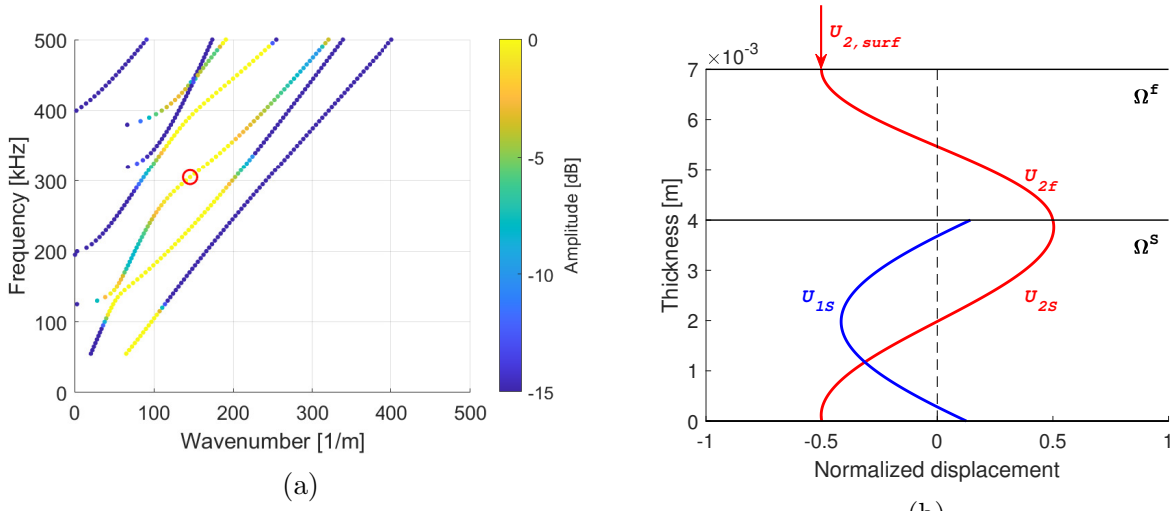


FIG. 2. (a) Guided modes dispersion curves with their frequency dependent excitability computed by SAIGA for a 2D cortical bone plate of 4mm ($\rho = 2310$ kg/m$^3$, $C_P = 2900$ m/s, $C_S = 1600$ m/s) overlaid with 3mm soft tissue layer ($\rho^f = 1010$ kg/m$^3$, $C^f = 1400$ m/s). The color scale shows the excitability of each mode in dB normalized to the mode with the highest excitability at each frequency. (b) Mode shape of the selected mode (red circle on (a)).

pursuit of this objective, a cost function was formulated to ascertain the optimal fit between the experimental curves and a particular instantiation of the simulated dataset. This method offers a systematic way to estimates the cortical bone properties of the plates. The accuracy and robustness of this approach depends on several factors including the accuracy of the SAIGA method, the quality of the experimental dispersion curves and the choice of the cost function.

### *1. Cost Function*

A cost function serves as a metric to evaluate the precision of a particular model in capturing the inherent associations within a dataset. A pronounced disparity between predictions and actual outcomes leads to an elevated value of the cost function, while more accurate estimations correspond to reduced values. It represents the foundation for solving an inverse problem. The choice of the cost function can influence the performance of an inversion. It is important to use a function that represents the type of problem and the distribution of data. Using excitability enable to add information about the amplitude of the guided wave mode propagating in the model in addition with their dispersive trajectories in the frequency against wavenumber plot. Consequently, the cost function was designed to measure the difference of amplitude between experimental and simulated dispersion curves as shown in Fig. 3.

For a given set of parameters $\Lambda$=($\rho$ $E$ $\nu$ $h^S$ $\rho^f$ $C^f$ $h^f$), the amplitude difference at each frequency is given by:

$$d_n(\Lambda, f) = Ex(k_n(\Lambda), f) - A(k_n(\Lambda), f) \tag{6}$$

where $Ex(k_n(\Lambda), f)$ is the excitability of mode $k_n(\Lambda)$ of the simulated dispersion curves, $A(k_n(\Lambda), f)$ is the experimental amplitude observed at wavenumber $k_n$ for the same frequency. Examples of distances $d_n$ can be observed on Fig. 3(c).

To ensure that the inversion is based on modes with the highest amplitudes, a weighting factor $\chi_n$ is calculated as the excitability of a given mode divided by the maximum excitability of modes for each frequency[46]. This ensures higher amplitude modes play a dominant

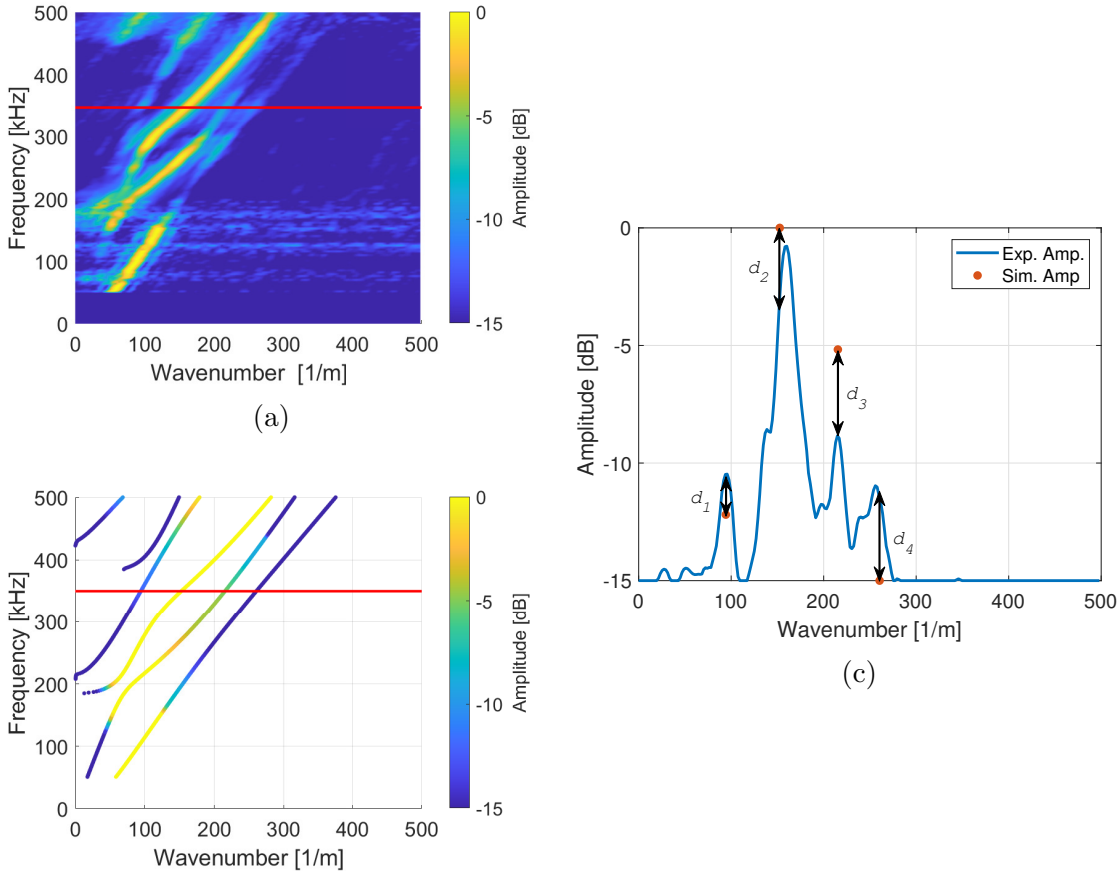


FIG. 3. (a) Surface plot representing experimental dispersion curves. (b) Simulated dispersion curves with mode excitability computed with SAIGA. (c) Projection of experimental amplitude at 350 kHz and simulated excitability at the same frequency, showing the distance measured for the calculation of the cost function.

role in the inversion process.

$$\chi_n(\Lambda, f) = \frac{Ex(k_n(\Lambda), f) - \xi}{-\xi} \tag{7}$$

where $N$ is the total number of simulated modes for a given frequency. $\xi$ is a user defined threshold setting the weighting factor equal to zero if the excitability of a given mode is inferior or equal to it. For example, by observing Fig. 3(c) which depicts distances between

simulated and experimental dispersion curves at 350 kHz, with a threshold $\xi = -15\ dB$, the weighting factor $\chi_4 = 0$ as the excitability of the fourth mode is equal to $\xi$. For the other modes, we have $\chi_1 = 0.19$, $\chi_2 = 1.0$ as it's the higher amplitude mode, and $\chi_3 = 0.66$.

The cost function for a set of parameters $J(\Lambda)$ is then calculated as follow:

$$J(\Lambda) = \sum_{f} \sqrt{\sum_{n=1}^{N} (d_n(\Lambda, f) \times \chi_n(\Lambda, f))^2} \tag{8}$$

Such a cost function will therefore consider high amplitude modes and neglect those with an amplitude below the threshold. Doing so reduces the risk of using irrelevant information in the inversion and the solution can be considered as more accurate.

### *2. Parameters sweeping*

To minimize the cost function and find the best fit between experimental and simulated data, the cost function was calculated for every model by sweeping each parameter along a multidimensional grid. Range of parameters were chosen to cover properties of both plates. This enables to test the effectiveness of our methodology in distinguishing between a bone in a healthy state and one afflicted by osteoporosis. Table I represents the set of parameters. Each range of parameters was defined large enough to ensure the measured properties from the plates are far enough from the range limits.

The grid steps were determined by balancing resolution fidelity and computational efficiency. For the whole dataset, the total number of cases was 72 600. To ascertains the robustness of our method, each parameter within the model was subject to variation, encompassing both values inside and outside the experimentally determined uncertainty range

TABLE I. Range of model parameters and their respective step used to perform the inversion.

| | Parameters range | Step |
|---|---|---|
| $\rho$ (kg/m$^3$) | [2050-2550] | 50 |
| $E$ (GPa) | [11-21] | 1 |
| $\nu$ | [0.23-0.26] | 0.01 |
| $h^S$ (mm) | [3.25-5.25] | 0.5 |
| $\rho^f$ (kg/m$^3$) | 1000 | 1 |
| $C^f$ (m/s) | [1275-1525] | 50 |
| $h^f$ (mm) | [1.6-2.4] | 0.2 |

of measured properties (see section II C 1 and III A). Based on the study of Mast[65], showing that density of soft tissue in the human body is comprised between 950 kg/m$^3$ and 1100 kg/m$^3$, the choice was made to keep the soft tissue density $\rho^f$ constant and equal to 1000 kg/m$^3$. As it will be shown in the results, the density of the soft tissue has virtually no effect on the dispersion curves. Emphasizing the significance of capturing all mode features, a frequency resolution increment of 5 kHz was selected, enabling 90 frequencies over the whole range of frequency [50 kHz – 500 kHz]. To counterbalance the computational demands inherent to such high-resolution, a comprehensive database encapsulating all possible model parameter combinations was constructed over an extended, continuous modeling session lasting less than 48 hours, demonstrating the effectiveness of the SAIGA method.

The pre-existing database was utilized to calculate the cost function values within the 6-D space, eliminating the need to rerun the model for every subsequent optimization scenario.

## C. Experimental Measurements

### *1. Cortical Bone Phantom Plates*

The measurements were performed with two cortical bone phantom plates layered with soft tissue mimicking material provided by True Phantom Solutions (Windsor, ON, Canada). One plate has material properties reflecting a healthy cortical bone and the other has properties similar to an osteoporotic bone. Both plates have the same material for the soft tissue layer. They have the same dimension: 15x15 mm with approximately 4 mm of cortical layer and 2 mm of soft tissue. Pulse-echo measurements were performed to acquire reference values for sound velocity in each layer which will be used in comparison with those obtained by the inversion. To do so, longitudinal and shear single element piezoelectric probes were used (Olympus V125-RM and Olympus V154-RM respectively). Small samples of each plate were cut and used to measure the density of each layer. To do so, the sample was weighted and its volume measure with a 3D laser scanner (Absolute Arm 85) from Hexagon (Stockholm, Sweden). The measurement uncertainty of density is subsequently derived from the relative uncertainties of the measuring instruments. The thicknesses of the samples were measured 20 times and pulse-echo measurements were then performed the same number of times to measure velocities. Then, 20 pulse-echo measurements were realized at different locations over the rest of the phantom plates to estimate the true thickness of each layer. Assumption

was made concerning the quasi-isotropic properties of the layers. However, it appeared that the thicknesses of the layers were not homogeneous all over the plates, with 15% to 20% variation for the cortical layers, and around 10% for the soft tissue layers. Therefore, mean values will be used to compared with the results obtained by the inversion.

### *2. Axial Transmission Measurements*

A proprietary ultrasonic probe was specifically built to perform ultrasonic excitation. The probe had a central frequency of 400 kHz with a -6 dB bandwidth between 200 kHz and 600 kHz approximately. Elements of the probe were specifically chosen to maximize the emission of ultrasonic waves through soft tissue and cortical bone. The device was in contact with the upper part of the soft tissue layer and coupled with an ultrasonic gel Ultragel® II. A series of several Hann windowed tonebursts were used as input waveform, with central frequencies varying between 50 kHz and 500 kHz with a step of 50 kHz. The number of cycles evolved with the central frequencies to keep a bandwidth of 50 kHz for each toneburst. Four consecutive acquisitions were realized on the plates (two in the length-width directions and the two along the diagonals, see Fig. 1(b)) along the direction of propagation at 60 positions equally spaced by 1 mm using a laser Doppler vibrometer (Polytech OFV-505). The probe was repositioned between each acquisition. Raw data were processed using the 2D Fast Fourier Transform[66], enabling the extraction of experimental dispersion curves for each of the four acquisitions with the intensities of the propagating modes in a frequency-wavenumber diagram.

## III. RESULTS

### A. Phantom Plates Properties Measurement

Due to uncertainties regarding the geometrical and material properties of the phantom plates, pulse-echo measurements were performed to determine the reference values of sound velocity and thickness of each layer. The plates were assumed homogeneous such that material properties and densities were measured on small samples of each layer. The same material was used for the soft tissue layer of both plates. As mentioned previously, it is worth noted that a discrepancy between 10% and 20% is observed for the different layer thicknesses over the whole surface of the plates. This can be explained by the method of fabrication of the plates. Table II summarizes the reference properties of each layer.

### B. Effect of the soft tissue density

A study was conducted on the soft tissue parameters while maintaining other properties at a constant level. Subsequently, the maximal normalized cost function value was compared with the minimal value ($J(\Lambda) = 1$) corresponding to the best fit scenario. In accordance with Mast[65] and other relevant studies[67], the parameter range for the soft tissue density $\rho^f$ was defined to be between 900 kg/m$^3$ to 1200 kg/m$^3$. The ranges for $C^f$ and $h^f$ are respectively [1250-1550] m/s and [1.0-2.5] mm. The study was performed on the healthy plate and each parameter can take 31 values.

Examining the outcomes yielded by altering solely the soft tissue density $\rho^f$, the normalized cost function pertaining to the least favorable fitting scenario registers at $J_{max}(\Lambda_{\rho^f}) =$

TABLE II. Bone Phantom Plates Properties.

| | Healthy Cortical Layer | Osteo. Cortical Layer | Soft Tissue Layer |
|---|---|---|---|
| $\rho$ (kg/m$^3$) | $2416 \pm 16$ | $2139 \pm 14$ | $977 \pm 12$ |
| $C_P$ (m/s) | $3000 \pm 115$ | $2655 \pm 65$ | $1390 \pm 90$ |
| $C_S$ (m/s) | $1755 \pm 50$ | $1530 \pm 35$ | - |
| $h^S$ (mm) | $4.3 \pm 0.7$ | $4.3 \pm 0.8$ | - |
| | Soft Tissue Healthy Plate | Soft Tissue Osteo. Plate | |
| $h^f$ (mm) | $2.0 \pm 0.2$ | $2.1 \pm 0.2$ | - |

1.086. In contrast, the normalized cost function values for the least favorable fittings when altering solely the soft tissue velocity $C^f$ or the soft tissue thickness $h^f$ stand at $J_{max}(\Lambda_{C^f}) = 2.260$ and $J_{max}(\Lambda_{h^f}) = 2.948$, respectively. Furthermore, upon examining the qualitative impact on the simulated dispersion curves (Fig. 4), $\rho^f$ does not exert a substantial influence on the trajectory of high-amplitude modes when contrasted with $C^f$ and $h^f$, where variations in these parameters notably affect the modes of significance. Therefore, fixing the soft tissue density can be considered as having virtually no effect on the inversion results but reduces the parameter exploration in the fitting. The decision was taken to set the soft tissue density $\rho^f$ as a constant in our sweeping parameters.

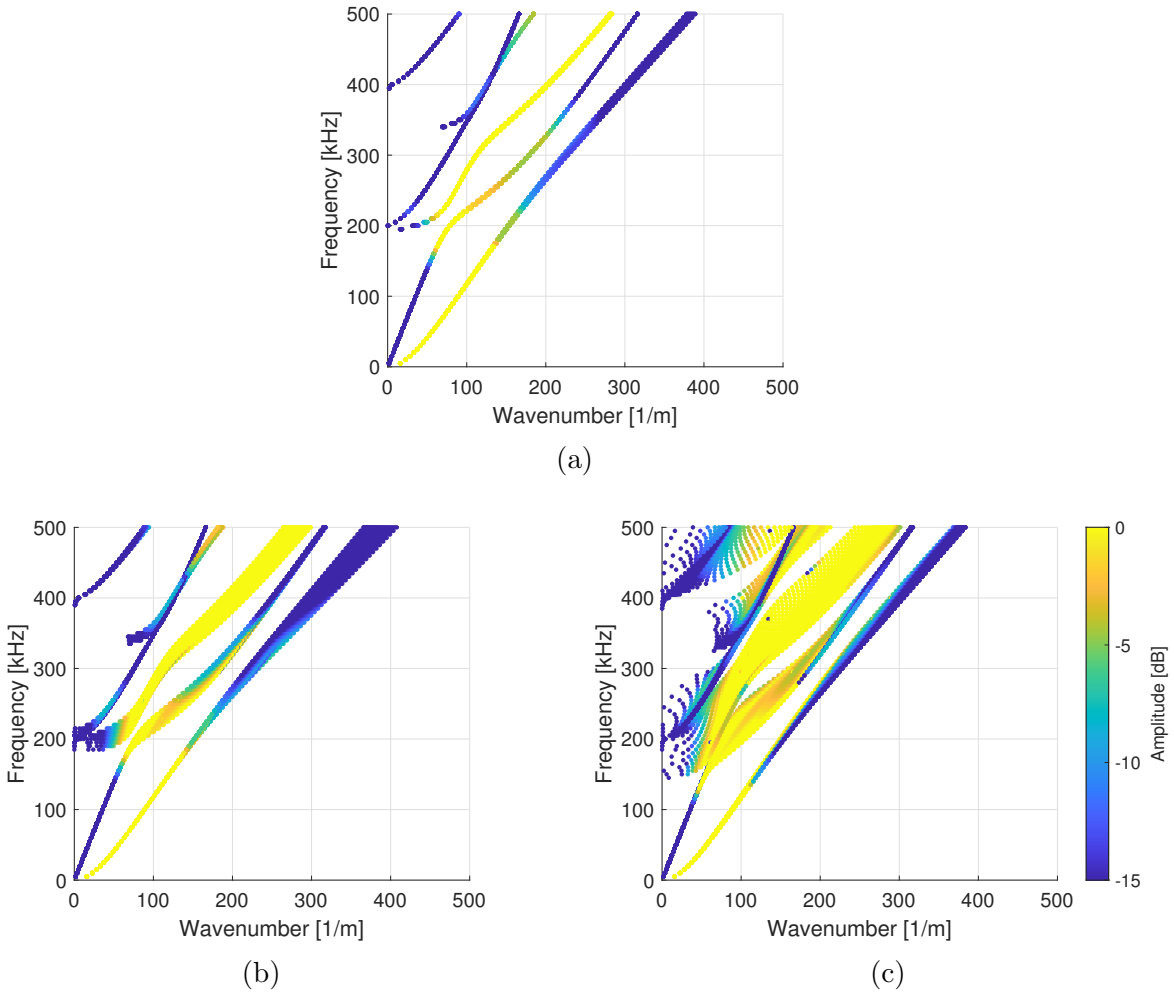


(a)

(b)

(c)

FIG. 4. Influence of property variations on the trajectory of ultrasonic modes: (a) soft tissue density $\rho^f$, (b) wave velocity in soft tissue $C^f$, and (c) thickness of the soft tissue $h^f$.

### C. Fitting of Simulated Data

As previously mentioned, four acquisitions were conducted for each plate along various directions to measure experimental dispersion curves. The inversion procedure was executed for both plates to determine the optimal set of parameters from the database. Fig. 5(a-b) illustrates the most favorable outcomes achieved through the proposed method. Semi-analytical predictions are depicted as points overlaying the experimental surface plot. The

experimental plots depicted herein are the result of averaging the 2D-FFT plots obtained from the four separate axial transmission measurements. This approach aims to consolidate spatial frequency information across multiple measurements for enhanced clarity in visual analysis. The alignment of experimental and simulated dispersion curves demonstrates a highly satisfactory agreement, with all high excitability modes perfectly matched. A threshold of -15dB was established to mitigate the impact of noise in experimental measurements, facilitating clearer dispersion curves and facilitating a more straightforward fitting process. Furthermore, the attenuation of modes in the simulated data closely aligns with the attenuation observed experimentally.

### D. Estimated Properties

The mean of the inverse characteristics over the four axial transmission measurements corresponding to the optimal fitting of each plate are detailed in Table III, alongside reference properties and associated relative errors. The findings indicate a strong agreement in property values, revealing errors under 2.0% for the cortical layers. However, a more notable margin is observed for the soft tissue thickness, with errors up to 5%. The soft tissue layer thickness is not uniform along the plates. Additionally, the pulse-echo measurements introduce the potential for inaccuracies, as the layers may undergo compression during the assessment.

Fig. 5(c-d) illustrates the inverted values in conjunction with the reference properties and their respective uncertainties. The derived values are obtained through the averaging of the reciprocals acquired from individual measurements across the four axial transmission

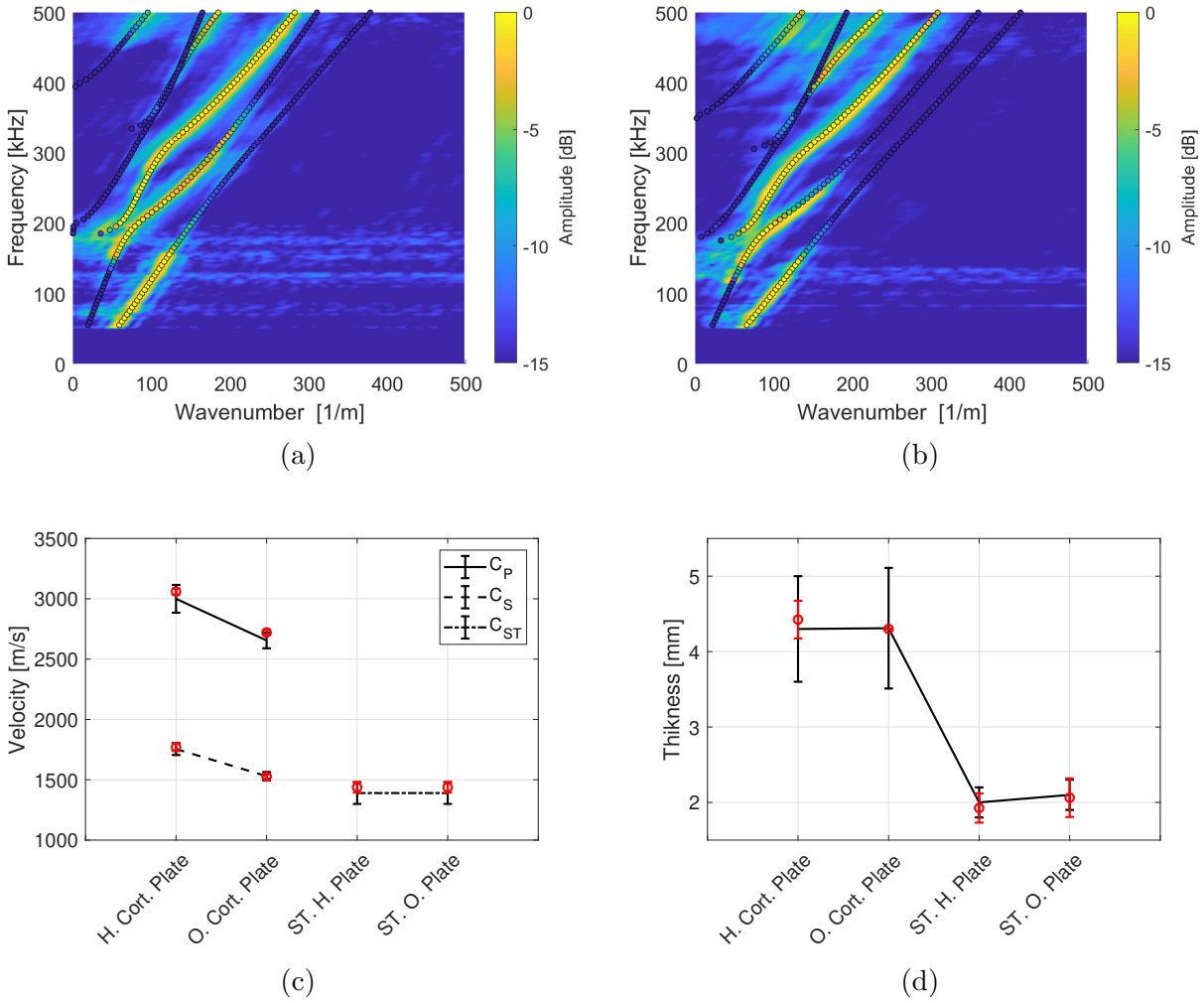


FIG. 5. Optimal fitting results between experimental and simulated dispersion curves for (a) healthy phantom plate, and (b) osteoporotic phantom plate. Average inverse values in conjunction with the reference properties and their respective uncertainties, (c) velocity properties, (d) thickness properties.

scenarios. Associated uncertainties are represented by their respective standard deviations. Each inverse value falls within the uncertainty range of its corresponding property.

TABLE III. Average Inverse Properties of Phantom Plates with their Relative Errors.

| | Healthy Plate | | | Osteo. Plate | | |
|---|---|---|---|---|---|---|
| | Ref. | Inv. | Err.% | Ref. | Inv. | Err.% |
| $C_P$ (m/s) | $3000 \pm 115$ | $3052 \pm 30$ | 1.74 | $2655 \pm 65$ | $2653 \pm 82$ | 0.07 |
| $C_S$ (m/s) | $1755 \pm 50$ | $1755 \pm 29$ | 0.02 | $1530 \pm 35$ | $1508 \pm 45$ | 1.39 |
| $h^S$ (mm) | $4.30 \pm 0.7$ | $4.40 \pm 0.25$ | 1.74 | $4.30 \pm 0.8$ | $4.25 \pm 0.0$ | 1.16 |
| | Soft Tissue Healthy Plate | | | Soft Tissue Osteo. Plate | | |
| $C^f$ (m/s) | $1390 \pm 90$ | $1437 \pm 25$ | 3.42 | $1390 \pm 90$ | $1437 \pm 48$ | 3.42 |
| $h^f$ (mm) | $2.00 \pm 0.2$ | $1.95 \pm 0.3$ | 2.50 | $2.10 \pm 0.2$ | $2.00 \pm 0.16$ | 4.76 |

### *1. Estimated Bulk-Velocities*

Fig. 5(c) displays the mean and standard deviation obtained for longitudinal and shear velocities in the cortical layer of both plates, as well as the wave velocities in their corresponding soft tissue layer (red circles), alongside the reference average values obtained by pulse-echo measurement (black lines). The predicted values fell within the uncertainty range of the reference values for both plates, and their associated standard deviations were of a comparable range to the reference ones. It is worth remembering that ultrasonic pulse-echo measurements were conducted across the plates (dimension of 150 x 150 mm), and the four axial transmission measurements were taken along a 60 mm length at four different locations (two diagonals and two perpendicular axes). Therefore, the predicted values approximately

represent the average values across the plates, as well as the reference values. The error was found to be less than 2% for cortical velocities and up to 3.4% for soft tissue velocity. However, the average inverted values of the soft tissue velocity were found to be equal for both plates, suggesting that the reference velocity of the soft tissue layer may have been underestimated during pulse-echo measurement. Changes in the experimental environment could have resulted in slight variations in the properties of the soft tissue sample, accounting for this minor difference.

### *2. Estimated Thicknesses*

Fig. 5(d) shows the comparison between the estimated thickness of each layer (red circles) and their corresponding reference values (black lines). Similar to the velocities, a very good agreement can be observed between the predicted and reference values. However, as explained in section III A, the thickness values of each layer were not homogeneous over the plates, which leads to uncertainties in the reference thicknesses measured by pulse-echo measurement. Regarding the cortical phantom layer, these reference values can be interpreted as the equivalent thickness across the entire plate area. Analogous to an *in-vivo* radius, the predicted thickness represents an averaged thickness over the entire volume corresponding to the investigated region of interest. Axial transmission measurements reflect the mean thickness along the propagation direction. Four axial transmission measurements were conducted in four different directions, each separated by 45 degrees, yielding a predicted thickness that corresponds to the mean actual thickness of the plate. Inverse properties were found to be close enough to the reference values to exhibit an error of less than 2% for the

cortical thicknesses and 5% for the soft tissue layers but remains in the standard deviation of the reference values.

## IV. DISCUSSION

The cost function value was computed across the multidimensional model grid, successfully identifying a global minimum for each acquisition and sample within the cost function map. Sweeping through six dimensions is notably computationally intensive. Even when using SAIGA, which enables a case calculation within a few seconds, it requires approximatively 48 hours to run through the 72 600 scenarios. However, leveraging the existing database enabled a gradual reduction in grid calculations to just a few minutes. Sweeping the model parameters across a finite set (rather than employing an optimization search routine) ensures that the global minimum is attained at each acquisition without needing additional verification or concern regarding the optimization search's performance and control variables.

### A. Assessment of Cortical Layer Density

Despite the promising match observed between the experimental data and the simulated model, uncertainties persist regarding local minima. Upon investigation of cortical density, the inverse values for the healthy cortical plate and the osteoporotic cortical plate are $2237 \pm 165$ kg/m$^3$ and $2337 \pm 221$ kg/m$^3$, respectively, with errors of 7.4% and 9.3% compared to reference values. Through analysis of the distribution of cost function values for experimental axial transmission measurement #4 on both plates (see Fig. 6), a local minimum can be

identified for each density in our parameter set. These local minima remain very close to each other, with a maximal normalized cost function of $J_{max}(\Lambda_\rho) = 1.097$, an no visual differences can be seen between each solution. These uncertainties may arise concerning the inverted properties.

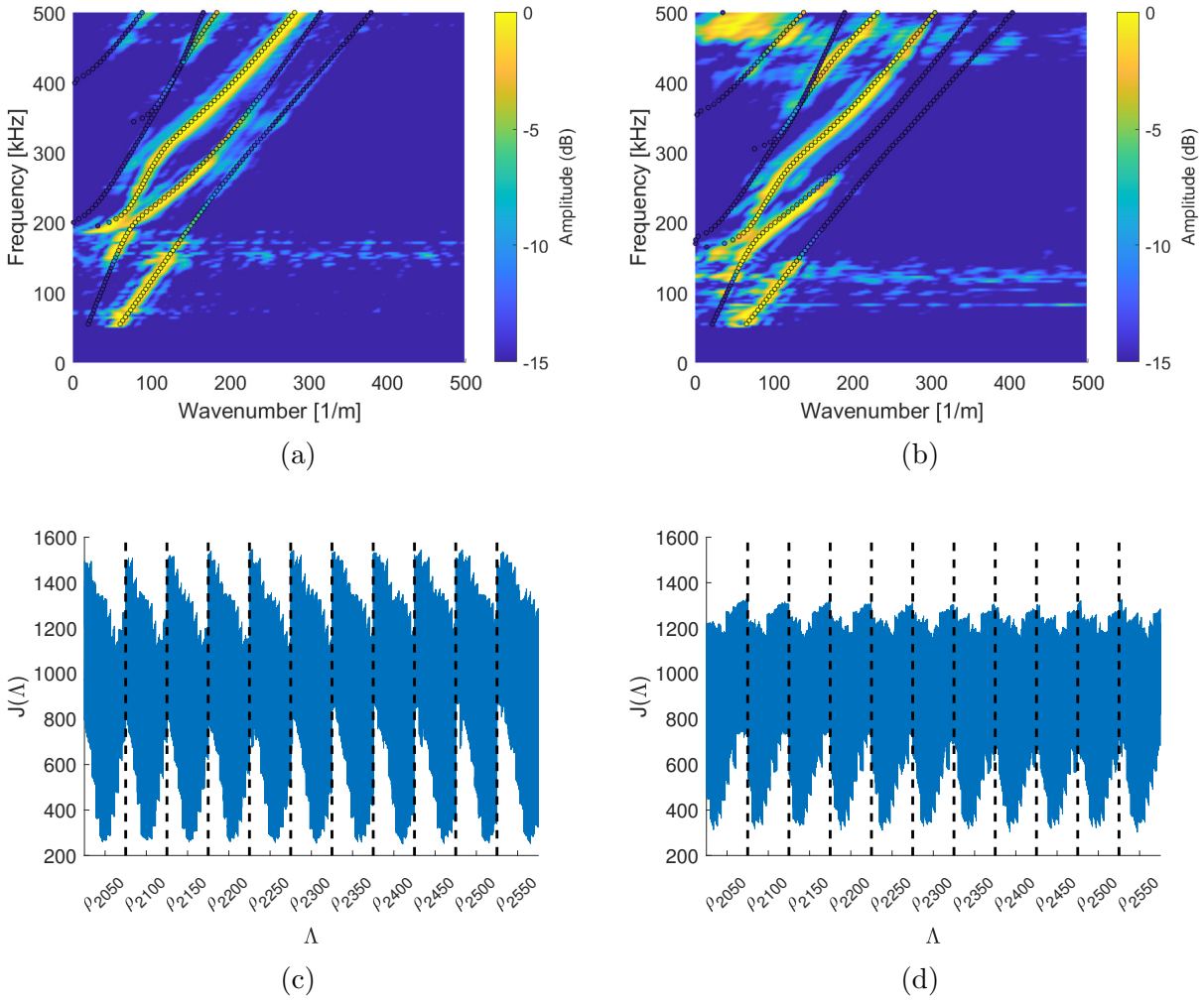


FIG. 6. Optimal fitting results between experimental axial transmission measurement #4 and simulated dispersion curves for (a) healthy phantom plate, and (b) osteoporotic phantom plate. Distribution of the cost function values with the corresponding density for experimental axial transmission measurement #4 (c) on the healthy plate and (d) on the osteoporotic plate.

However, upon inspection of the inverted cortical properties at each density (from 2050 kg/m$^3$ to 2550 kg/m$^3$), the inverse values of longitudinal and shear velocities remain nearly unchanged, along with a significant portion of the other parameters, except for the Young's modulus (refer to Table IV). These phenomena can be elucidated by the reciprocal adjustment of the density and the Young's modulus, which serve to attain longitudinal and shear velocities consistent with the experimental dispersion curves. Moreover, looking at our range of parameters $\rho = [2050 : 50 : 2550]$ kg/m$^3$ and $E = [11 : 1 : 21]$ GPa, for a constant Poisson coefficient $\nu = 0.26$, target velocities can be obtained through a large number of pairs $(\rho - E)$ as shown on Fig. 7.

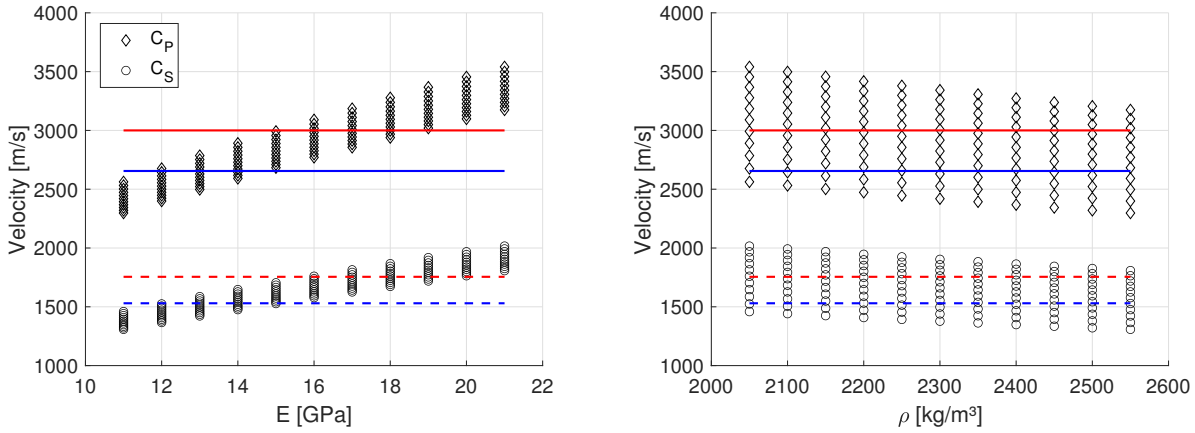


(a) (b)

FIG. 7. Longitudinal and shear velocities possible values obtained through the set of parameters express as a function of (a) the Young's modulus $E$ for different values of the density $\rho$, (b) the density $\rho$ for different values of $E$. Red lines represent the reference values of $C_P$ (full line) and $C_S$ (dote line) for the healthy plate and blue lines for the osteoporotic plate.

As shown in Table IV, density and Young's modulus compensate each other to achieve the correct velocities. The higher the density, the higher the Young's modulus, for a given

TABLE IV. Mean inverted cortical properties for each frequency, relative to the optimal fit identified for axial transmission measurement #4.

| | Healthy Plate Meas. #4 | | | Osteo. Plate Meas. #4 | | |
|---|---|---|---|---|---|---|
| | Best fit Meas. #4 | Mean over densities | Var.% $(\sigma/ref)$ | Best fit Meas. #4 | Mean over densities | Var.% $(\sigma/ref)$ |
| $\rho$ (kg/m$^3$) | 2400 | $2300 \pm 166$ | 6.90 | 2550 | $2300 \pm 166$ | 6.51 |
| $C_P$ (m/s) | 3030 | $3023 \pm 26$ | 0.86 | 2683 | $2675 \pm 29$ | 1.08 |
| $C_S$ (m/s) | 1725 | $1722 \pm 15$ | 0.87 | 1528 | $1523 \pm 16$ | 1.05 |
| $h^S$ (mm) | 4.25 | $4.25 \pm 0.0$ | 0.00 | 4.25 | $4.25 \pm 0.0$ | 0.00 |
| $E$ (GPa) | 18.0 | $17.2 \pm 1.3$ | 7.22 | 15 | $13.4 \pm 1.0$ | 6.67 |
| $\nu$ | 0.26 | $0.26 \pm 0.0$ | 0.00 | 0.26 | $0.26 \pm 0.0$ | 0.00 |

value of the Poisson coefficient. Consequently, the proposed method cannot directly assess the density of the cortical layer.

However, several studies have demonstrated the possibility of obtaining bone density through mathematical models[53,68,69]. By adapting the work of Vu[53] and Pereira[46] for use with the phantom plate material used in this study, it is possible to estimate $\rho$ from the bulk velocities.

For a 2D isotropic plate, the elasticity coefficients are given by $C_{11} = \rho C_P^2$, $C_{33} = \rho C_S^2$, $C_{12} = C_{11} - 2C_{33}$. Using experimental pulse-echo measurement values, a linear interpola-

tion can be made to express $C_{11}$, $C_{12}$ and $C_{33}$ as a function of the density. Consequently, longitudinal and shear bulk velocities can be expressed as functions of density (Fig. 8). This enables the determination of density for both plates corresponding to the inverse velocities depicted in Table III. The results yield $\rho = 2445 \pm 35$ kg/m$^3$ and $\rho = 2130 \pm 14$ kg/m$^3$ for the healthy plates and the osteoporotic plate, respectively, with relative errors of 1.2% and 0.4%.

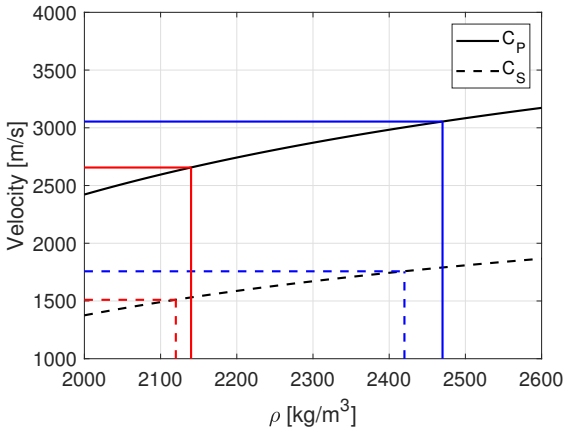


FIG. 8. Bulk velocities varying with the bulk density, derived from the values of the elastic properties for an isotropic medium adapting from the homogenization theory introduced in[53] and used in[46] to the phantom material. (Blue lines) Inverse values for longitudinal and shear velocities of Healthy phantom plate. (Red lines) Inverse values for longitudinal and shear velocities of Osteoporotic phantom plate.

## B. Importance of Excitability

Utilizing excitability inherently prolongs computation time for each scenario, necessitating the calculation of mode shape for every mode at each frequency across all parameters

sets. Nonetheless, excitability guarantees the consideration of all modes exhibiting high amplitudes. Upon examining visually results from simulated datasets without the application of excitability, it becomes evident that inversion biases towards modes with high amplitudes across a broad frequency spectrum while overlooking modes of lower amplitudes. Consequently, certain modes are entirely disregarded, resulting in reduced thickness values and elevated velocities. As illustrated in Fig. 9, the second mode consistently disappears from the simulated curves. As depicted in Table V, the inverse values demonstrate an error exceeding 15% in comparison to the reference properties. Notably, several simulation parameters, particularly the thickness of cortical and soft tissue layers, approach the lower bounds of their respective ranges.

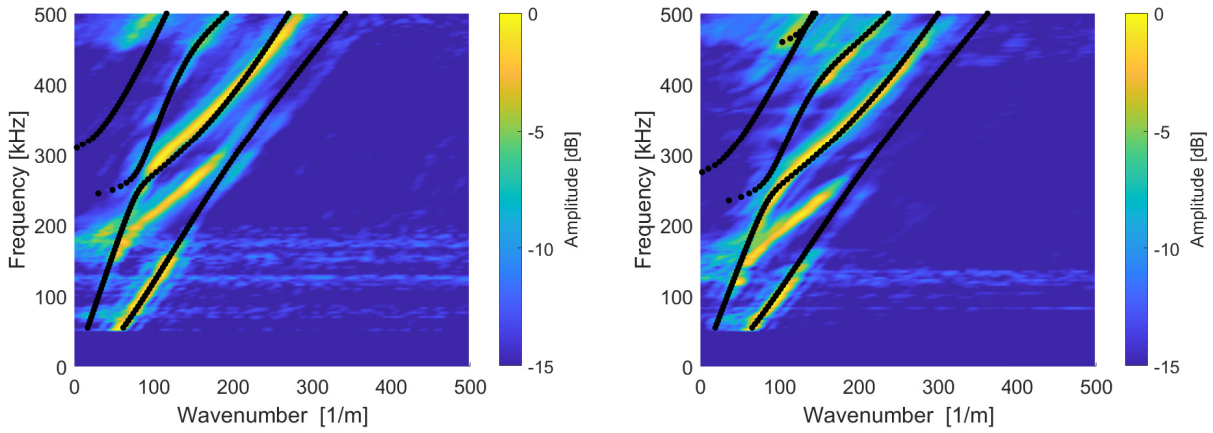


(a) (b)

FIG. 9. Optimal fitting results between experimental and simulated dispersion curves without excitability for (a) healthy phantom plate, and (b) osteoporotic phantom plate.

TABLE V. Average Inverse Properties of Phantom Plates with their Relative Errors without using the excitability in the inversion scheme.

| | Healthy Plate | | | Osteo. Plate | | |
|---|---|---|---|---|---|---|
| | Ref. | Inv. | Err.% | Ref. | Inv. | Err.% |
| $C_P$ (m/s) | $3000 \pm 115$ | $3475 \pm 0.0$ | 15.83 | $2655 \pm 65$ | $3064 \pm 52$ | 15.39 |
| $C_S$ (m/s) | $1755 \pm 50$ | $2032 \pm 0.0$ | 15.81 | $1530 \pm 35$ | $1785 \pm 39$ | 16.09 |
| $h^S$ (mm) | $4.30 \pm 0.7$ | $3.25 \pm 0.0$ | 24.42 | $4.30 \pm 0.8$ | $3.25 \pm 0.0$ | 24.42 |
| | Soft Tissue Healthy Plate | | | Soft Tissue Osteo. Plate | | |
| $C^f$ (m/s) | $1390 \pm 90$ | $1487 \pm 75$ | 7.01 | $1390 \pm 90$ | $1500 \pm 29$ | 7.91 |
| $h^f$ (mm) | $2.00 \pm 0.2$ | $1.7 \pm 0.2$ | 15.00 | $2.10 \pm 0.2$ | $1.6 \pm 0.0$ | 23.81 |

## V. CONCLUSION

In this study, the inverse characterization of two cortical phantom plates covered with a layer of soft tissue was conducted at low frequencies (between 50 and 500kHz). The study focuses on the estimation of five parameters: longitudinal velocity, shear velocity, and thickness of the cortical layer, as well as velocity and thickness of the soft tissue layer. The proposed SAIGA model successfully aligned the amplitude in the experimental dispersion curves by utilizing a combination of multiple high excitability mode segments.

The integration of modal excitability into the cost function played a pivotal role in the inversion procedure, substantially reducing the number of relevant modes. This reduction was

achieved by assigning weights to the modes based on their excitabilities. The incorporation of a limited number of modes prevents misfit of the data during the inversion process.

A high level of agreement was observed between the inversely determined properties of cortical properties (bulk velocities and thickness) and their corresponding reference values obtained through experimental measurements, with errors consistently below 2.0%. The surrounding soft-tissue layer is critical during the inversion procedure due to the high number of modes involved. The model introduced in this study successfully extracted these parameters even when a layer of soft tissue was present atop the cortical plate. Despite a slightly larger error (inferior to 5%) in the determination of the soft tissue characteristics, other properties remained accurately retrieved.

Additionally, the proposed low-frequency axial transmission configuration demonstrated its efficacy in deducing equivalent bone properties within a multi-layer model. Remarkably, this approach required fewer modes compared to conventional inversion techniques that utilize higher frequencies. The current method serves as a promising proof of concept and serves as a valuable reference for the development of a customized array probe, which could be deployed for a comprehensive acquisition and reception in future extensive *in-vivo* and clinical investigations. A portable device incorporating this specific probe could be utilized in clinical settings for routine bone quality assessments, facilitating the early diagnosis of osteoporosis at a reduced cost compared to DEXA or QCT-Scan technologies. However, a significant challenge lies in developing a probe with a sufficiently wide bandwidth to capture low-frequency guided waves propagating along the radius. Moreover, a dedicated design of the setup will be required to ensure the repeatability of the location of the probe compared

to the radius. Furthermore, a clinical study will be necessary to compare the device's results with reference values obtained through X-ray imaging. This comparison will help establish a set of indicators representative of bone health, that can be used by practitioners for diagnostic purposes.

The proposed method uses low-frequency ultrasonic guided waves to evaluate the bone at the organ scale, while high frequency devices approximate bone by a plate-like structure. The present study demonstrates the method's capability to accurately retrieve the properties of a cortical phantom plate topped by a soft tissue layer, thus serving as a proof of concept. Consequently, this model will evolve into a radius-shaped model, filled with bone marrow and surrounded by soft tissue, following the work of Seyfaddini et al.[48]. The computational methodology using SAIGA for simulations will remain unchanged. To accurately represent the bone cortex, the model will transition from an isotropic material to a transverse isotropic medium[18,46]. In such a model, it will be necessary to use a homogenization scheme to determine the elastic stiffness coefficients as a function of the bone's porosity/density, as described in the literature[53,70,71]. Additionally, the inverse scheme could evolve to by using AI techniques to enhance its robustness, which will assess bone properties based on the dispersive trajectories and amplitudes of guided wave modes propagating in the waveguide.

## ACKNOWLEDGMENTS

The authors would like to thank Nvidia for providing us with an Nvidia Quadro P6000 graphics card for our GPU simulations. This research was funded by Natural Sciences and Engineering Research Council of Canada: NSERC – RGPIN – 2020 – 05802. The authors

511 acknowledge the support of the Laboratoire Franco-Canadien de Recherches Ultrasonores
512 (LAFCUS).

## 513 AUTHOR DECLARATIONS

### 514 Conflict of Interest

515 The authors have no conflicts to disclose.

## 516 DATA AVAILABILITY

517 The data that support the findings of this study are available from the corresponding
518 author upon reasonable request.

## 519 REFERENCES

520 [1]W. H. Organization, *Assessment of fracture risk and its application to screening for post-*
521 *menopausal osteoporosis : report of a WHO study group [meeting held in Rome from*
522 *22 to 25 June 1992]* (World Health Organization, 1994), https://apps.who.int/iris/
523 handle/10665/39142.

524 [2]W. H. Organization, *Guidelines for preclinical evaluation and clinical trials in osteoporosis*
525 (World Health Organization, 1998), https://apps.who.int/iris/handle/10665/42088.

526 [3]N. Bochud, Q. Vallet, J.-G. Minonzio, and P. Laugier, "Predicting bone strength with
527 ultrasonic guided waves," Scientific Reports **7**(1), 43628 (2017) https://www.nature.
528 com/articles/srep43628 doi: 10.1038/srep43628.

[4]P. Laugier and G. Haïat, eds., *Bone Quantitative Ultrasound* (Springer Netherlands, Dordrecht, 2011), http://link.springer.com/10.1007/978-94-007-0017-8.

[5]P. Laugier and Q. Grimal, eds., *Bone Quantitative Ultrasound: New Horizons*, Vol. 1364 of *Advances in Experimental Medicine and Biology* (Springer International Publishing, Cham, 2022), https://link.springer.com/10.1007/978-3-030-91979-5.

[6]C. Cooper, G. Campion, and L. J. Melton, "Hip fractures in the elderly: A world-wide projection," Osteoporosis International **2**(6), 285–289 (1992) http://link.springer.com/10.1007/BF01623184 doi: 10.1007/BF01623184.

[7]J. A. Kanis, O. Johnell, A. Oden, B. Jonsson, C. De Laet, and A. Dawson, "Risk of hip fracture according to the World Health Organization criteria for osteopenia and osteoporosis," Bone **27**(5), 585–590 (2000) https://www.sciencedirect.com/science/article/pii/S8756328200003811 doi: 10.1016/S8756-3282(00)00381-1.

[8]L. J. Melton, E. A. Chrischilles, C. Cooper, A. W. Lane, and B. L. Riggs, "How Many Women Have Osteoporosis?," Journal of Bone and Mineral Research **20**(5), 886–892 (2005) https://asbmr.onlinelibrary.wiley.com/doi/abs/10.1359/jbmr.2005.20.5.886 doi: 10.1359/jbmr.2005.20.5.886.

[9]A. Randell, P. N. Sambrook, T. V. Nguyen, H. Lapsley, G. Jones, P. J. Kelly, and J. A. Eisman, "Direct clinical and welfare costs of osteoporotic fractures in elderly men and women," Osteoporosis International **5**(6), 427–432 (1995) http://link.springer.com/10.1007/BF01626603 doi: 10.1007/BF01626603.

[10]S. R. Cummings, D. B. Karpf, F. Harris, H. K. Genant, K. Ensrud, A. Z. LaCroix, and D. M. Black, "Improvement in spine bone density and reduction in risk of vertebral fractures during treatment with antiresorptive drugs," The American Journal of Medicine **112**(4), 281–289 (2002) https://www.sciencedirect.com/science/article/pii/S000293430101124X doi: 10.1016/S0002-9343(01)01124-X.

[11]O. Johnell, J. A. Kanis, A. Odén, I. Sernbo, I. Redlund-Johnell, C. Petterson, C. De Laet, and B. Jönsson, "Mortality after osteoporotic fractures," Osteoporosis International **15**(1), 38–42 (2004) http://link.springer.com/10.1007/s00198-003-1490-4 doi: 10.1007/s00198-003-1490-4.

[12]K. Engelke, C. Libanati, Y. Liu, H. Wang, M. Austin, T. Fuerst, B. Stampa, W. Timm, and H. K. Genant, "Quantitative computed tomography (QCT) of the forearm using general purpose spiral whole-body CT scanners: Accuracy, precision and comparison with dual-energy X-ray absorptiometry (DXA)," Bone **45**(1), 110–118 (2009) https://www.sciencedirect.com/science/article/pii/S8756328209012472 doi: 10.1016/j.bone.2009.03.669.

[13]N. Li, X.-m. Li, L. Xu, W.-j. Sun, X.-g. Cheng, and W. Tian, "Comparison of QCT and DXA: Osteoporosis Detection Rates in Postmenopausal Women," International Journal of Endocrinology **2013**, e895474 (2013) https://www.hindawi.com/journals/ije/2013/895474/ doi: 10.1155/2013/895474 publisher: Hindawi.

[14]W. Kalender, K. Engelke, T. P. Fuerst, C.-C. Glüer, P. Laugier, and J. Shepherd, "Quantitative Aspects of Bone Densitometry:: Contents," Journal of the ICRU **9**(1), NP.2–NP (2009) https://academic.oup.com/jicru/article-lookup/doi/10.1093/jicru/

ndp014 doi: 10.1093/jicru/ndp014.

[15]C.-C. Glüer, "Quantitative Ultrasound Techniques for the Assessment of Osteoporosis: Expert Agreement on Current Status," Journal of Bone and Mineral Research **12**(8), 1280–1288 (1997) https://asbmr.onlinelibrary.wiley.com/doi/abs/10.1359/jbmr.1997.12.8.1280 doi: 10.1359/jbmr.1997.12.8.1280.

[16]Q. Grimal, J. Grondin, S. Guérard, R. Barkmann, K. Engelke, C.-C. Glüer, and P. Laugier, "Quantitative ultrasound of cortical bone in the femoral neck predicts femur strength: results of a pilot study," Journal of Bone and Mineral Research: The Official Journal of the American Society for Bone and Mineral Research **28**(2), 302–312 (2013) doi: 10.1002/jbmr.1742.

[17]J.-G. Minonzio, M. Talmant, and P. Laugier, "Guided wave phase velocity measurement using multi-emitter and multi-receiver arrays in the axial transmission configuration," The Journal of the Acoustical Society of America **127**(5), 2913–2919 (2010) http://asa.scitation.org/doi/10.1121/1.3377085 doi: 10.1121/1.3377085.

[18]N. Bochud, Q. Vallet, Y. Bala, H. Follet, J.-G. Minonzio, and P. Laugier, "Genetic algorithms-based inversion of multimode guided waves for cortical bone characterization," Physics in Medicine and Biology **61**(19), 6953–6974 (2016) https://iopscience.iop.org/article/10.1088/0031-9155/61/19/6953 doi: 10.1088/0031-9155/61/19/6953.

[19]D. Pereira, A. Le Duff, G. Painchaud-April, and P. Belanger, "Simulation-Based Inversion for the Characterization of Adhesively Bonded Joints Using Ultrasonic Guided Waves," IEEE Transactions on Ultrasonics, Ferroelectrics, and Frequency Control **69**(7), 2400–2407

(2022) https://ieeexplore.ieee.org/document/9776578/ doi: 10.1109/TUFFC.2022.3175773.

[20]M. Asif, M. A. Khan, S. Z. Khan, R. S. Choudhry, and K. A. Khan, "Identification of an effective nondestructive technique for bond defect determination in laminate composites—A technical review," Journal of Composite Materials **52**(26), 3589–3599 (2018) http://journals.sagepub.com/doi/10.1177/0021998318766595 doi: 10.1177/0021998318766595.

[21]K. Heller, L. Jacobs, and J. Qu, "Characterization of adhesive bond properties using Lamb waves," NDT & E International **33**(8), 555–563 (2000) https://linkinghub.elsevier.com/retrieve/pii/S0963869500000220 doi: 10.1016/S0963-8695(00)00022-0.

[22]S. I. Rokhlin, B. Xie, and A. Baltazar, "Quantitative ultrasonic characterization of environmental degradation of adhesive bonds," Journal of Adhesion Science and Technology **18**(3), 327–359 (2004) http://www.tandfonline.com/doi/abs/10.1163/156856104773635463 doi: 10.1163/156856104773635463.

[23]M. Ponschab, D. A. Kiefer, and S. J. Rupitsch, "Simulation-Based Characterization of Mechanical Parameters and Thickness of Homogeneous Plates Using Guided Waves," IEEE Transactions on Ultrasonics, Ferroelectrics, and Frequency Control **66**(12), 1898–1905 (2019) doi: 10.1109/TUFFC.2019.2933699 conference Name: IEEE Transactions on Ultrasonics, Ferroelectrics, and Frequency Control.

[24]L. Bai, K. Xu, D. Li, D. Ta, L. H. Le, and W. Wang, "Fatigue evaluation of long cortical bone using ultrasonic guided waves," Journal of Biomechanics **77**, 83–90 (2018) http:

//www.sciencedirect.com/science/article/pii/S0021929018304469 doi: 10.1016/j.jbiomech.2018.06.015.

[25]A. Guha, M. Aynardi, P. Shokouhi, and C. J. Lissenden, "Identification of long-range ultrasonic guided wave characteristics in cortical bone by modelling," Ultrasonics **114**, 106407 (2021) https://linkinghub.elsevier.com/retrieve/pii/S0041624X21000482 doi: 10.1016/j.ultras.2021.106407.

[26]R. Barkmann, E. Kantorovich, C. Singal, D. Hans, H. K. Genant, M. Heller, and C.-C. Glüer, "A New Method for Quantitative Ultrasound Measurements at Multiple Skeletal Sites: First Results of Precision and Fracture Discrimination," Journal of Clinical Densitometry **3**(1), 1–7 (2000) https://www.sciencedirect.com/science/article/pii/S1094695006601261 doi: 10.1385/JCD:3:1:001.

[27]M. Muller, P. Moilanen, E. Bossy, P. Nicholson, V. Kilappa, J. Timonen, M. Talmant, S. Cheng, and P. Laugier, "Comparison of three ultrasonic axial transmission methods for bone assessment," Ultrasound in Medicine & Biology **31**(5), 633–642 (2005) https://www.sciencedirect.com/science/article/pii/S030156290500089X doi: 10.1016/j.ultrasmedbio.2005.02.001.

[28]C. F. Njeh, I. Saeed, M. Grigorian, D. L. Kendler, B. Fan, J. Shepherd, M. McClung, W. M. Drake, and H. K. Genant, "Assessment of bone status using speed of sound at multiple anatomical sites," Ultrasound in Medicine & Biology **27**(10), 1337–1345 (2001) https://www.sciencedirect.com/science/article/pii/S0301562901004379 doi: 10.1016/S0301-5629(01)00437-9.

[29]M. Talmant, S. Kolta, C. Roux, D. Haguenauer, I. Vedel, B. Cassou, E. Bossy, and P. Laugier, "In vivo Performance Evaluation of Bi-Directional Ultrasonic Axial Transmission for Cortical Bone Assessment," Ultrasound in Medicine & Biology **35**(6), 912–919 (2009) https://www.sciencedirect.com/science/article/pii/S030156290800598X doi: 10.1016/j.ultrasmedbio.2008.12.008.

[30]M. Sasso, G. Haiat, M. Talmant, P. Laugier, and S. Naili, "Singular value decomposition-based wave extraction in axial transmission: application to cortical bone ultrasonic characterization [correspondence]," IEEE Transactions on Ultrasonics, Ferroelectrics and Frequency Control **55**(6), 1328–1332 (2008) http://ieeexplore.ieee.org/document/4536927/ doi: 10.1109/TUFFC.2008.795.

[31]G. Haïat, S. Naili, Q. Grimal, M. Talmant, C. Desceliers, and C. Soize, "Influence of a gradient of material properties on ultrasonic wave propagation in cortical bone: Application to axial transmission," The Journal of the Acoustical Society of America **125**(6), 4043–4052 (2009) https://pubs.aip.org/jasa/article/125/6/4043/788436/Influence-of-a-gradient-of-material-properties-on doi: 10.1121/1.3117445.

[32]D. Hans, L. Genton, S. Allaoua, C. Pichard, and D. O. Slosman, "Hip Fracture Discrimination Study," Journal of Clinical Densitometry **6**(2), 163–172 (2003) https://linkinghub.elsevier.com/retrieve/pii/S1094695006602667 doi: 10.1385/JCD:6:2:163.

[33]K. M. Knapp, K. M. Knapp, G. M. Blake, T. D. Spector, and I. Fogelman, "Multisite Quantitative Ultrasound: Precision, Age- and Menopause-Related Changes, Fracture Discrimination, and T-score Equivalence with Dual-Energy X-ray Absorptiometry," Osteoporosis International **12**(6), 456–464 (2001) http://link.springer.com/10.1007/

s001980170090 doi: 10.1007/s001980170090.

[34]J.-G. Minonzio, J. Foiret, P. Moilanen, J. Pirhonen, Z. Zhao, M. Talmant, J. Timonen, and P. Laugier, "A free plate model can predict guided modes propagating in tubular bone-mimicking phantoms," The Journal of the Acoustical Society of America **137**(1), EL98–EL104 (2015) https://pubs.aip.org/jasa/article/137/1/EL98/912467/A-free-plate-model-can-predict-guided-modes doi: 10.1121/1.4903920.

[35]P. Moilanen, P. H. Nicholson, V. Kilappa, S. Cheng, and J. Timonen, "Assessment of the cortical bone thickness using ultrasonic guided waves: Modelling and in vitro study," Ultrasound in Medicine & Biology **33**(2), 254–262 (2007) https://linkinghub.elsevier.com/retrieve/pii/S0301562906017807 doi: 10.1016/j.ultrasmedbio.2006.07.038.

[36]R. M. Zebaze, A. Ghasem-Zadeh, A. Bohte, S. Iuliano-Burns, M. Mirams, R. I. Price, E. J. Mackie, and E. Seeman, "Intracortical remodelling and porosity in the distal radius and post-mortem femurs of women: a cross-sectional study," The Lancet **375**(9727), 1729–1736 (2010) https://linkinghub.elsevier.com/retrieve/pii/S0140673610603200 doi: 10.1016/S0140-6736(10)60320-0.

[37]P. Moilanen, P. Nicholson, V. Kilappa, S. Cheng, and J. Timonen, "Measuring guided waves in long bones: Modeling and experiments in free and immersed plates," Ultrasound in Medicine & Biology **32**(5), 709–719 (2006) https://linkinghub.elsevier.com/retrieve/pii/S0301562906014566 doi: 10.1016/j.ultrasmedbio.2006.02.1402.

[38]P. Moilanen, "Ultrasonic guided waves in bone," IEEE Transactions on Ultrasonics, Ferroelectrics and Frequency Control **55**(6), 1277–1286 (2008) http://ieeexplore.ieee.org/

677 document/4536922/ doi: 10.1109/TUFFC.2008.790.

678 [39]D. Ta, W. Wang, Y. Wang, L. H. Le, and Y. Zhou, "Measurement of the Dispersion and At-
679 tenuation of Cylindrical Ultrasonic Guided Waves in Long Bone," Ultrasound in Medicine
680 & Biology **35**(4), 641–652 (2009) https://linkinghub.elsevier.com/retrieve/pii/
681 S0301562908004808 doi: 10.1016/j.ultrasmedbio.2008.10.007.

682 [40]D. Pereira, G. Haiat, J. Fernandes, and P. Belanger, "Simulation of acoustic guided wave
683 propagation in cortical bone using a semi-analytical finite element method," The Journal
684 of the Acoustical Society of America **141**(4), 2538–2547 (2017) https://asa.scitation.
685 org/doi/full/10.1121/1.4979695 doi: 10.1121/1.4979695 publisher: Acoustical Soci-
686 ety of America.

687 [41]J. Foiret, J.-G. Minonzio, C. Chappard, M. Talmant, and P. Laugier, "Combined esti-
688 mation of thickness and velocities using ultrasound guided waves: a pioneering study on
689 in vitro cortical bone samples," IEEE Transactions on Ultrasonics, Ferroelectrics, and
690 Frequency Control **61**(9), 1478–1488 (2014) https://ieeexplore.ieee.org/document/
691 6882946 doi: 10.1109/TUFFC.2014.3062.

692 [42]J. Chen, J. Foiret, J.-G. Minonzio, M. Talmant, Z. Su, L. Cheng, and P. Laugier,
693 "Measurement of guided mode wavenumbers in soft tissue–bone mimicking phantoms
694 using ultrasonic axial transmission," Physics in Medicine and Biology **57**(10), 3025–
695 3037 (2012) https://iopscience.iop.org/article/10.1088/0031-9155/57/10/3025
696 doi: 10.1088/0031-9155/57/10/3025.

[43]T. N. Tran, L. Stieglitz, Y. J. Gu, and L. H. Le, "Analysis of Ultrasonic Waves Propagating in a Bone Plate over a Water Half-Space with and without Overlying Soft Tissue," Ultrasound in Medicine & Biology **39**(12), 2422–2430 (2013) https://linkinghub.elsevier.com/retrieve/pii/S0301562913008181 doi: 10.1016/j.ultrasmedbio.2013.06.007.

[44]P. Moilanen, M. Talmant, V. Kilappa, P. Nicholson, S. Cheng, J. Timonen, and P. Laugier, "Modeling the impact of soft tissue on axial transmission measurements of ultrasonic guided waves in human radius," The Journal of the Acoustical Society of America **124**(4), 2364–2373 (2008) https://doi.org/10.1121/1.2973228 doi: 10.1121/1.2973228.

[45]Y. Li, K. Xu, Y. Li, F. Xu, D. Ta, and W. Wang, "Deep Learning Analysis of Ultrasonic Guided Waves for Cortical Bone Characterization," IEEE Transactions on Ultrasonics, Ferroelectrics, and Frequency Control 1–1 (2020) doi: 10.1109/TUFFC.2020.3025546 conference Name: IEEE Transactions on Ultrasonics, Ferroelectrics, and Frequency Control.

[46]D. Pereira, J. Fernandes, and P. Belanger, "Ex Vivo Assessment of Cortical Bone Properties Using Low-Frequency Ultrasonic Guided Waves," IEEE Transactions on Ultrasonics, Ferroelectrics, and Frequency Control **67**(5), 910–922 (2020) doi: 10.1109/TUFFC.2019.2958035 conference Name: IEEE Transactions on Ultrasonics, Ferroelectrics, and Frequency Control.

[47]F. Seyfaddini, H. Nguyen-Xuan, and V.-H. Nguyen, "A semi-analytical isogeometric analysis for wave dispersion in functionally graded plates immersed in fluids," Acta Mechanica **232**(1), 15–32 (2021) https://link.springer.com/10.1007/s00707-020-02818-0 doi: 10.1007/s00707-020-02818-0.

[48]F. Seyfaddini, H. Nguyen-Xuan, and V.-H. Nguyen, "Wave dispersion analysis of three-dimensional vibroacoustic waveguides with semi-analytical isogeometric method," Computer Methods in Applied Mechanics and Engineering **385**, 114043 (2021) https://linkinghub.elsevier.com/retrieve/pii/S0045782521003741 doi: 10.1016/j.cma.2021.114043.

[49]M. Muller, D. Mitton, P. Moilanen, V. Bousson, M. Talmant, and P. Laugier, "Prediction of bone mechanical properties using QUS and pQCT: Study of the human distal radius," Medical Engineering & Physics **30**(6), 761–767 (2008) https://www.sciencedirect.com/science/article/pii/S1350453307001579 doi: 10.1016/j.medengphy.2007.08.006.

[50]J.-Y. Rho, L. Kuhn-Spearing, and P. Zioupos, "Mechanical properties and the hierarchical structure of bone," Medical Engineering & Physics **20**(2), 92–102 (1998) https://www.sciencedirect.com/science/article/pii/S1350453398000071 doi: 10.1016/S1350-4533(98)00007-1.

[51]V. Sansalone, S. Naili, V. Bousson, C. Bergot, F. Peyrin, J. Zarka, J. D. Laredo, and G. Haïat, "Determination of the heterogeneous anisotropic elastic properties of human femoral bone: From nanoscopic to organ scale," Journal of Biomechanics **43**(10), 1857–1863 (2010) https://www.sciencedirect.com/science/article/pii/S002192901000179X doi: 10.1016/j.jbiomech.2010.03.034.

[52]A. Sarvazyan, "Elastic Properties of Soft Tissues," in *Handbook of Elastic Properties of Solids, Liquids, and Gases*, Vol. Volume III : Elastic Properties of Solids: Biological and Organic Materials (Academic Press, 2001).

[53]M.-B. Vu and T. Nguyen-Sy, "On the effective anisotropic elastic properties of porous hydroxyapatite, porous collagen, and cortical bone: A homogenization scheme with percolation threshold concept," Mathematics and Mechanics of Solids **24**(4), 1091–1102 (2019) https://doi.org/10.1177/1081286518769961 doi: 10.1177/1081286518769961 publisher: SAGE Publications Ltd STM.

[54]D. A. Chrisman and M. Buras, "THE DYNAMIC MECHANICAL PROPERTIES OF HUMAN SKIN IN I/IV0," Journal of Biomechanics **16**(6), 365–372 (1983).

[55]J.-G. Minonzio, N. Bochud, Q. Vallet, Y. Bala, D. Ramiandrisoa, H. Follet, D. Mitton, and P. Laugier, "Bone cortical thickness and porosity assessment using ultrasound guided waves: An ex vivo validation study," Bone **116**, 111–119 (2018) https://linkinghub.elsevier.com/retrieve/pii/S8756328218302862 doi: 10.1016/j.bone.2018.07.018.

[56]J. Wu and F. Cubberley, "Measurement of velocity and attenuation of shear waves in bovine compact bone using ultrasonic spectroscopy," Ultrasound in Medicine & Biology **23**(1), 129–134 (1997) https://linkinghub.elsevier.com/retrieve/pii/S0301562996001846 doi: 10.1016/S0301-5629(96)00184-6.

[57]M. Sasso, G. Haïat, Y. Yamato, S. Naili, and M. Matsukawa, "Dependence of ultrasonic attenuation on bone mass and microstructure in bovine cortical bone," Journal of Biomechanics **41**(2), 347–355 (2008) https://www.sciencedirect.com/science/article/pii/S0021929007003776 doi: 10.1016/j.jbiomech.2007.09.001.

[58]S. Naili, M.-B. Vu, Q. Grimal, M. Talmant, C. Desceliers, C. Soize, and G. Haïat, "Influence of viscoelastic and viscous absorption on ultrasonic wave propagation in cortical

760 bone: Application to axial transmission," The Journal of the Acoustical Society of Amer-
761 ica **127**(4), 2622–2634 (2010) http://asa.scitation.org/doi/10.1121/1.3353091 doi:
762 10.1121/1.3353091.

763 [59]D. ROYER and E. Dieulesaint, *Elastic Waves in Solids I: Free and Guided Propagation*
764 (Springer Science & Business Media, 1999) google-Books-ID: SzwQ1UYspyQC.

765 [60]Z. A. B. Ahmad, J. M. Vivar-Perez, and U. Gabbert, "Semi-analytical finite element
766 method for modeling of lamb wave propagation," CEAS Aeronautical Journal **4**(1),
767 21–33 (2013) http://link.springer.com/10.1007/s13272-012-0056-6 doi: 10.1007/
768 s13272-012-0056-6.

769 [61]W. Karunasena, A. H. Shah, and S. K. Datta, "Wave Propagation in a Multilayered
770 Laminated Cross-Ply Composite Plate," Journal of Applied Mechanics **58**(4), 1028–
771 1032 (1991) https://asmedigitalcollection.asme.org/appliedmechanics/article/
772 58/4/1028/423315/Wave-Propagation-in-a-Multilayered-Laminated doi: 10.1115/
773 1.2897678.

774 [62]M. V. Predoi, M. Castaings, B. Hosten, and C. Bacon, "Wave propagation along trans-
775 versely periodic structures," The Journal of the Acoustical Society of America **121**(4),
776 1935–1944 (2007) http://asa.scitation.org/doi/10.1121/1.2534256 doi: 10.1121/
777 1.2534256.

778 [63]L. Piegl and W. Tiller, *The NURBS Book* (Springer Science & Business Media, 1996)
779 google-Books-ID: 7dqY5dyAwWkC.

[64]D. Starkey, "NURBS: Non-Uniform Rational B-Splines" (2009), https://www.cs.montana.edu/courses/spring2009/525/dslectures/NURBS.pdf.

[65]T. D. Mast, "Empirical relationships between acoustic parameters in human soft tissues," Acoustics Research Letters Online **1**(2), 37–42 (2000) https://pubs.aip.org/asa/arlo/article/1/2/37-42/123603 doi: 10.1121/1.1336896.

[66]D. Alleyne and P. Cawley, "A two-dimensional Fourier transform method for the measurement of propagating multimode signals," The Journal of the Acoustical Society of America **89**(3), 1159–1168 (1991) http://asa.scitation.org/doi/10.1121/1.400530 doi: 10.1121/1.400530.

[67]M. O. Culjat, D. Goldenberg, P. Tewari, and R. S. Singh, "A Review of Tissue Substitutes for Ultrasound Imaging," Ultrasound in Medicine & Biology **36**(6), 861–873 (2010) https://linkinghub.elsevier.com/retrieve/pii/S030156291000075X doi: 10.1016/j.ultrasmedbio.2010.02.012.

[68]S. Nobakhti and S. J. Shefelbine, "On the Relation of Bone Mineral Density and the Elastic Modulus in Healthy and Pathologic Bone," Current Osteoporosis Reports **16**(4), 404–410 (2018) http://link.springer.com/10.1007/s11914-018-0449-5 doi: 10.1007/s11914-018-0449-5.

[69]T. S. Keller, Z. Mao, and D. M. Spengler, "Young's modulus, bending strength, and tissue physical properties of human compact bone," Journal of Orthopaedic Research **8**(4), 592–603 (1990) https://onlinelibrary.wiley.com/doi/abs/10.1002/jor.1100080416 doi: 10.1002/jor.1100080416 _eprint:

https://onlinelibrary.wiley.com/doi/pdf/10.1002/jor.1100080416.

[70]M. Granke, Q. Grimal, A. Saïed, P. Nauleau, F. Peyrin, and P. Laugier, "Change in porosity is the major determinant of the variation of cortical bone elasticity at the millimeter scale in aged women," Bone **49**(5), 1020–1026 (2011) https://linkinghub.elsevier.com/retrieve/pii/S8756328211011458 doi: 10.1016/j.bone.2011.08.002.

[71]W. J. Parnell, M. B. Vu, Q. Grimal, and S. Naili, "Analytical methods to determine the effective mesoscopic and macroscopic elastic properties of cortical bone," Biomechanics and Modeling in Mechanobiology **11**(6), 883–901 (2012) http://link.springer.com/10.1007/s10237-011-0359-2 doi: 10.1007/s10237-011-0359-2.